

Fault weakening and earthquake instability by powder lubrication

Ze'ev Reches¹ & David A. Lockner²

Earthquake instability has long been attributed to fault weakening during accelerated slip¹, and a central question of earthquake physics is identifying the mechanisms that control this weakening². Even with much experimental effort^{2–12}, the weakening mechanisms have remained enigmatic. Here we present evidence for dynamic weakening of experimental faults that are sheared at velocities approaching earthquake slip rates. The experimental faults, which were made of room-dry, solid granite blocks, quickly wore to form a fine-grain rock powder known as gouge. At modest slip velocities of 10–60 mm s⁻¹, this newly formed gouge organized itself into a thin deforming layer that reduced the fault's strength by a factor of 2–3. After slip, the gouge rapidly 'aged' and the fault regained its strength in a matter of hours to days. Therefore, only newly formed gouge can weaken the experimental faults. Dynamic gouge formation is expected to be a common and effective mechanism of earthquake instability in the brittle crust as (1) gouge always forms during fault slip^{5,10,12–20}; (2) fault-gouge behaves similarly to industrial powder lubricants²¹; (3) dynamic gouge formation explains various significant earthquake properties; and (4) gouge lubricant can form for a wide range of fault configurations, compositions and temperatures¹⁵.

The dynamic rupture of earthquakes requires a strength loss from pre-slip, static friction to co-seismic, dynamic friction, and so major experimental effort has been devoted to determining fault friction^{2–12}. The experimental results are frequently analysed in the formalism of rate- and state-friction^{2,3,6,9,11,13}. The adjustable parameters of this framework have successfully quantified the relations between friction variations (for example, weakening, strengthening, instability), and slip conditions (rock type, gouge, temperature, velocity, distance and 'aging')^{2,3,6,9,11,13}.

Rock friction is typically measured using saw-cuts of cylinders (triaxial geometry) or direct-shear geometry, in which rock blocks slide at low velocity (<0.1 mm s⁻¹) and over short distances (<30 mm)^{2,3,9–11}, or with rotary-shear devices, that allow for high slip velocity over long distances^{4,5}. Low-velocity experiments revealed weakening by time-dependent creep at contacting asperities on bare-rock surfaces², and grain rolling in a granular shear zone¹¹. High-velocity experiments revealed weakening by melting on rock surfaces⁴ or silica gel flow in quartz-rich rocks⁷. Fault gouge, the fine-grain rock powder that is found in almost all field faults^{13–16} and in laboratory experiments^{3,5,11,12}, was also recognized as controlling fault rheology during earthquakes¹⁷ and experiments^{3,5,10}.

The present study focuses on experimental evidence for the physical mechanisms of earthquake weakening at slip speeds approaching coseismic rates. The experiments show that the gouge layer is a dynamic component, the properties of which are continuously changing in response to velocity, slip distance, 'aging' and heat. We believe that these observations are consistent with a rate- and state-friction formulation but would require parameter values that differ from those determined for slow velocities. The gouge develops by wear from a strong, 'immature' state to a weak, 'mature', shear-activated state. Only a gouge layer that develops during slip lubricates and weakens the fault,

whereas preexisting gouge strengthens quickly (within days) and must be reactivated to lubricate the fault.

We developed a rotary apparatus specifically designed to simulate earthquake weakening on a laboratory fault that is comprised of two room-dry cylindrical rock blocks (Methods and Supplementary Information). We conducted hundreds of sliding tests on four samples of Sierra White granite with cumulative slip distance of up to 1,180 m per sample. In a typical run, the slip velocity V was increased or decreased in steps under constant normal stress σ_n . Each velocity step was maintained for a constant time interval (for example, 180 s) or a constant slip distance (1–2 m). Fault strength is reported as friction coefficient μ , the ratio of measured shear load to measured normal load. A quasi-steady-state friction coefficient was observed after slip of at least 1 m at constant velocity (Supplementary Information). We determined 254 friction-velocity values in 35 runs with increasing or decreasing velocity up to 1 m s⁻¹, and $\sigma_n = 0.5$ –7.1 MPa.

In a representative experiment, the sample was subjected to 31 velocity steps from $V = 0.002$ to 0.16 m s⁻¹, with $\sigma_n = 2.4$ MPa, about 1.1 m slip at each step and total slip of 35 m. The friction-velocity relationship (red curve in Fig. 1a) is characteristic of all runs (Fig. 1b). We recognize five friction-velocity regimes (Fig. 1b): (1) For $V < 0.003$ m s⁻¹, friction varies widely with $\mu = 0.45$ –0.95 between different runs, but is relatively stable in a given run. (2) For $V = 0.003$ –0.01 m s⁻¹, friction values are scattered and decrease to $\mu = 0.4$ –0.6 with increasing velocity. Friction may drop abruptly during a single velocity step. (3) For $V = 0.01$ –0.05 m s⁻¹, friction reaches a minimum of $\mu \approx 0.3$. (4) For $V = 0.05$ –0.25 m s⁻¹, friction rapidly rises up to $\mu = 0.80$. (5) For $V = 0.25$ –1.0 m s⁻¹, slip becomes unstable with stick-slip activity and sample failure; the few data points in this range suggest friction drop. The current friction reduction at $V = 0.001$ –0.05 m s⁻¹ was previously observed⁶ (Fig. 1b).

Each rock sample was surface ground, mounted in the loading frame and tested at room temperature and humidity (estimated as 23 °C and 40–60%, respectively). A thin gouge layer developed after slip distances of only a few millimetres, as commonly observed^{18–20}. The initial surface roughness was quickly modified by wear and gouge accumulation. When the sample blocks were separated, they displayed layers of fine-grain gouge that adhered to the sliding surfaces, forming a continuous coating (Fig. 2a–c). The gouge layer thickness was 100–300 μ m. The gouge was continuously created by wear of the rock surfaces and excess gouge was extruded (Fig. 2b).

The wear-rate of the experimental fault is reported here as the ratio of fault-normal closure to slip distance, in micrometres per metre (see Supplementary Information). In run 616, the total wear approaches 0.6 mm after 35 m slip (blue line in Fig. 1a), and the non-monotonic wear-rate is 4–12 μ m m⁻¹ (black line in Fig. 1a). We note the similarity between wear-rate and friction variations with slip velocity (Fig. 1a and Supplementary Information).

The fault surfaces after test 556 (run 3 s, $V = 0.97$ m s⁻¹ and $\sigma_n = 4.7$ MPa) exposed a slightly cohesive gouge layer with thickness 0.45 ± 0.15 mm. Scanning electron microscope (SEM) images of this gouge revealed that most grains are angular and in the submicrometre

¹School of Geology and Geophysics, University of Oklahoma, 100 East Boyd Street, Norman, Oklahoma, USA. ²US Geological Survey, 345 Middlefield Road, Menlo Park, California 94025, USA.

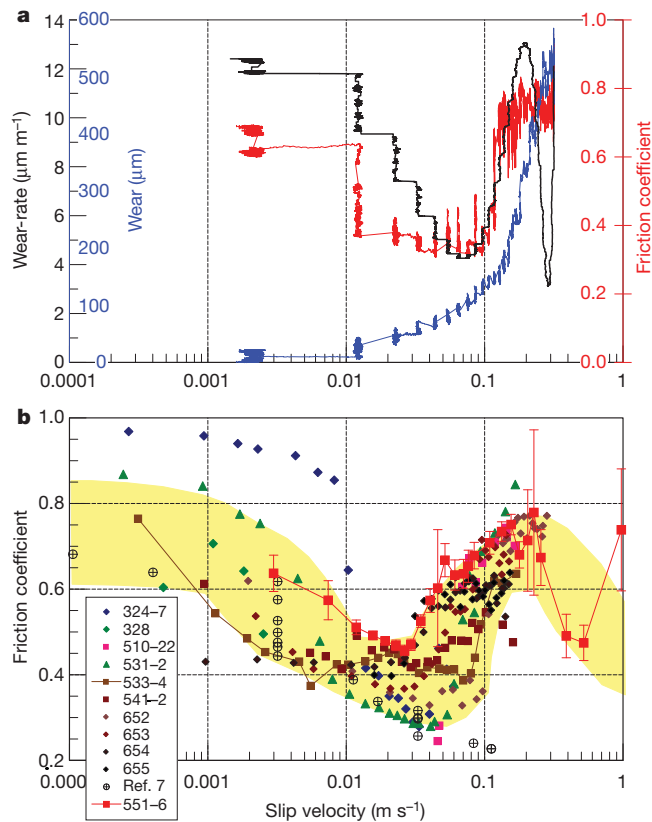


Figure 1 | Experimental friction-velocity relations in Sierra White granite samples. **a**, Friction (red), fault wear (blue), and wear-rate (black) in run 616 as function of slip velocity. Run includes 31 velocity steps from 0.002 to 0.16 m s⁻¹; ~1.1 m slip at each step; 35 m total slip; $\sigma_n = 2.4$ MPa. The wear-rate is explained in the online-only Methods. We notice similar trends in friction and wear-rate variations. **b**, Experimental friction coefficients for 35 runs (run numbers shown) with 254 values; each datum point is the average friction value at the velocity interval; standard deviation bars are shown only for one run for the sake of clarity; yellow shading bounds the data without outliers; data from ref. 7 also shown.

range (many grains are below the 0.1 μm SEM resolution; Fig. 2c). Also, partial-melt regions appeared with patches of glassy material that agglomerated submicrometre grains (Fig. 2d).

The fault temperature was measured by two thermocouples embedded at 3 mm and 6 mm from the sliding surface (Methods). Figure 3 displays friction versus thermocouple temperature in two tests of increasing velocity (final $V = 0.16$ m s⁻¹), and two tests of decreasing velocity (initial $V = 0.15$ m s⁻¹). Slip at each velocity step was 2.0 m, and $\sigma_n = 3.1$ MPa. Increasing velocity tests show an abrupt friction increase from $\mu \approx 0.37$ to 0.71 when the temperature was increased from 100 to 120 °C; a further increase to 470 °C had no additional effect. Decreasing-velocity tests show an approximately reverse pattern: roughly constant friction above ~200 °C and then weakening from $\mu \approx 0.60$ to 0.42 as the temperature dropped below 200 °C. (Our thermal model predicts a time-delay between fault and thermocouple: in an increasing-velocity test, the thermocouple temperature of 100–120 °C corresponds to a fault surface temperature of 130–150 °C, and in a decreasing-velocity test, 200 °C on the thermocouple corresponds to ~170 °C on the surface.)

These friction–temperature curves in Fig. 3 provide a clue to the micro-mechanism of gouge behaviour. If the abrupt friction transition occurs at a temperature of 130–150 °C, then the friction transition may indicate dehydration of gouge-adsorbed water during temperature increase, and water re-adsorption during temperature drop. We measured the amount and rates of water adsorption by heating three samples of gouge powder for 24 h at 210 °C, and then continuously

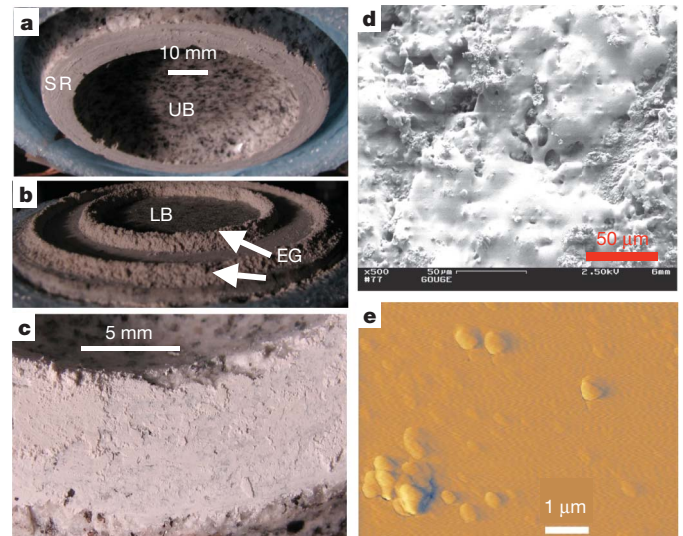


Figure 2 | Gouge formation during the experiments. **a**, **b**, Blocks of Sierra White granite after experiment 652. LB, lower block; UB, upper block; SR, sliding ring; EG, gouge ejected. Note adhered gouge coating on the sliding ring (**a**) and heaps of ejected gouge on the lower block (**b**). **c**, Close-up view of a sliding surface showing adhered gouge and gouge layer. **d**, SEM image with melted-like area in which glass ‘glues’ fine angular grains (test 556). **e**, Atomic force microscope image of gouge grains of test 670 on glass plate; note the submicrometre grains and agglomerated grains in the lower left corner.

weighing the powder while exposed to room humidity and temperature. The gouge adsorbed ~0.8% water within 15 s after removal from the oven, ~1.5% within 90 s and ultimately ~2% water. The present gouge has a Brunauer–Emmett–Teller surface area of ~16 m² g⁻¹. Thus, 1.5% of adsorbed water corresponds to an average thickness of 3 to 4 monomolecular layers. The adsorption and removal of this thin film drastically modified the macroscopic frictional properties of the gouge^{5,22} (Supplementary Information).

We also ran a series of slide–hold–slide experiments. In the initial run, the fault slid first at 0.046 m s⁻¹ for 600 s (brown curve in Fig. 4) to steady-state $\mu \approx 0.3$ after about 10 m slip, the fault was then held stationary for ~30 s. When sliding was resumed at the same velocity,

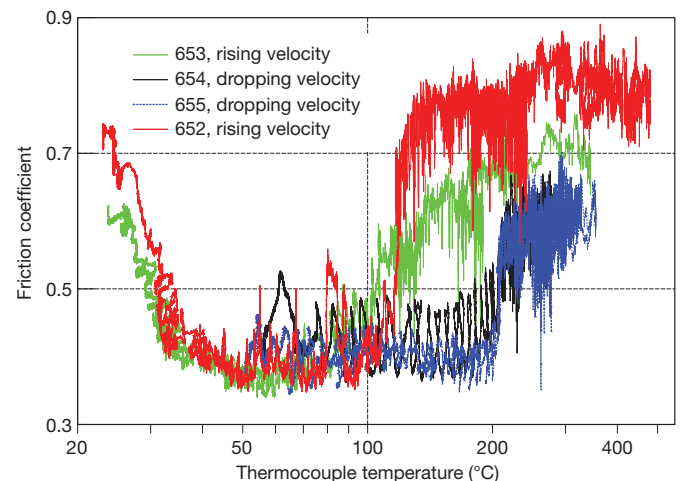


Figure 3 | Friction as function of the temperature measured by thermocouple located 3 mm from the sliding surface. The four tests were run under $\sigma_n = 3.1$ MPa. Increasing velocity steps (up to $V = 0.16$ m s⁻¹) were applied in two tests (652, 653) and decreasing steps (starting at $V = 0.15$ m s⁻¹) were applied in the two other tests (654, 655). We note drastic friction changes at 100–120 °C for increasing-velocity tests and at ~200 °C for decreasing-velocity tests.

a slight strength recovery was followed by weakening back to $\mu \approx 0.3$ (blue curve in Fig. 4). But when the sliding was resumed at a much lower velocity of $V = 0.0003 \text{ m s}^{-1}$ (green curve in Fig. 4), the friction increased to $\mu \approx 0.92$ within 600 s. Similar behaviour was observed for quartzite⁷, and time-dependent strengthening of fine-grained rock powder²³, and this behaviour has been incorporated in the ‘slowness’ law form of rate- and state-friction⁶. The present strength recovery reflects grain agglomeration (Fig. 2e), sintering (Fig. 2d), or recrystallization. Because strength recovery is active even during slip (green curve in Fig. 4), it may lead to self-healing of a slipping fault.

Different lines of evidence indicate that the new gouge, which formed during slip, controls friction in our experiments. First, because gouge accumulates from the onset of slip¹⁸ and adheres to fault surfaces (Figs 2a–c), it is always present during slip. Second, the 100–300- μm -thick gouge layer (Fig. 2c) eliminates asperity–asperity contacts, and the slip is accommodated within this layer. Third, the strength transition at $\sim 150^\circ\text{C}$ (Fig. 3) is consistent with a surface hydration–dehydration mechanism of fine-grained powder. Fourth, steady-state friction is achieved here after slip distances of 3–10 m (brown curve in Fig. 4), $\sim 1 \text{ m}$ in quartzite⁷, and $\sim 15 \text{ m}$ in gabbro⁵; these distances indicate that the steady state requires prolonged wear and gouge accumulation⁴ (Fig. 2). Fifth, the time-dependent strength recovery⁵ is common to fine-grained rock powders²³ with large surface area. Finally, the experiments show that friction and wear-rate vary similarly with slip velocity (Fig. 1a and Supplementary Information), and both are high at low velocities, low at intermediate velocities, and high again at high velocities. This inter-dependence of friction and wear-rate²⁴ implies that gouge formation and accumulation are linked to friction intensity.

Although our results may be quantified using rate- and state-friction^{2,13}, we choose to first present a physical, phenomenological description of the evolution of fault strength as it accelerates from rest to about 1 m s^{-1} . The preceding text suggests a five-stage process (Fig. 5): Stage (1) Initially, the fault includes bare surfaces (ground sample), or a healed gouge zone.

Stage (2) At low velocity, the friction and wear-rate are high (Fig. 1a), but only minor gouge amount is accumulated owing to the short slip distance and competing healing processes (Fig. 4).

Stage (3) Distinct fault weakening occurs at an intermediate velocity ($V = 0.01\text{--}0.05 \text{ m s}^{-1}$), when the gouge layer reaches a critical thickness and structure, resulting in low strength and wear-rate (Fig. 1).

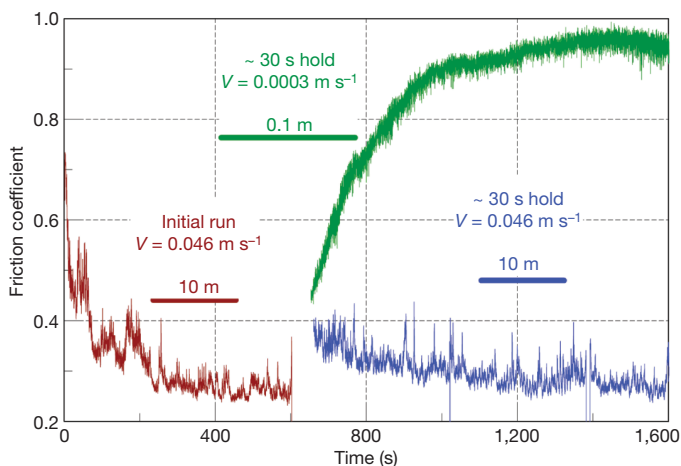


Figure 4 | Friction measurements in slide-hold-slide experiments. Initial shearing (0.046 m s^{-1} for 600 s, brown trace) produced steady-state friction of ~ 0.3 after $\sim 220 \text{ s}$ ($= 10 \text{ m}$), followed by hold (no slip) for $\sim 30 \text{ s}$. Then slip was restored, once at 0.046 m s^{-1} for 1,000 s (blue trace), and once at 0.0003 m s^{-1} (green trace). We note the initial small strength recovery after the 30 s hold-time for both consecutive runs. However, while the second run at 0.046 m s^{-1} subsequently weakened, the run at 0.0003 m s^{-1} continued to strengthen until steady-state friction of ~ 0.92 was achieved after $\sim 600 \text{ s}$ ($= 0.18 \text{ m}$).

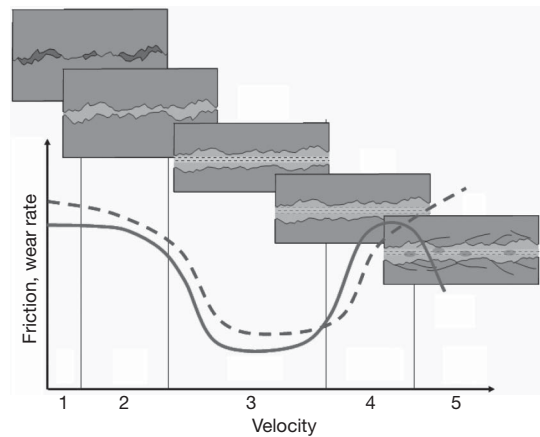


Figure 5 | Proposed model for fault weakening as it accelerates from rest to about 1 m s^{-1} . Friction variations are represented by the solid curve and wear-rate variations by the dashed curve; compare with Fig. 1a. Stage (1): the initial setting signifies bare surfaces or healed gouge. Stage (2): wear, initial gouge formation, no lubrication. Stage (3): cumulative wear, critical gouge layer and powder lubrication. Stage (4): strengthening (for example by dehydration). Stage (5): unstable slip, global failure. Each stage is pictured schematically.

Stage (4) The fine-grained gouge powder is highly reactive and may undergo temporal strengthening even during slip, for example, dehydration due to heating (Fig. 3) or agglomeration (Fig. 4).

Stage (5) Slip becomes unstable at high velocity ($0.25\text{--}1.0 \text{ m s}^{-1}$), ultimately leading to fracturing and failure of our granite sample.

Fault gouge is not the only fine-grained powder that reduces friction. Tribological investigations have shown similar behaviour for dry powders of graphite, MoS_2 , talc or quartz²¹. Part of the cohesive powder adheres to the solid blocks, while the remainder forms a ‘third body’ that flows and lubricates^{25–27}. We propose that rock gouge develops a ‘third body’ that separates the sliding blocks (Fig. 2c) and lubricates the fault.

The experimental results reported here are applicable to important issues of earthquake physics such as fault-weakening efficiency and non-seismic slip. Low-speed velocity-stepping experiments find that weakening typically develops within $\sim 10^{-5} \text{ m slip}^{2,9,11}$. In contrast, near-field seismic observations suggest that weakening distances are on the order of metres for large earthquakes²⁸. Weakening distances reported here and previously^{5,7} are from 1 to 10 m (Fig. 4) and may reflect weakening mechanisms (that is, gouge layer formation) that cannot be sampled by short-distance experiments. Furthermore, low-speed short-distance experiments have a very small rate-dependent strength loss: typical rates for quartzo-feldspathic rocks^{2,28,29} are $\partial\mu/\partial\ln V \approx -0.002$, whereas the weakening shown in Fig. 1 between 0.001 and 0.04 m s^{-1} is $\partial\mu/\partial\ln V \approx -0.1$. Thus, once the initial nucleation phase for an earthquake is complete and the fault accelerates to a modest velocity (for example, $\sim 0.05 \text{ m s}^{-1}$), gouge friction reduction is likely to take over and dominate fault weakening.

The present experiments provide a powerful concept for understanding earthquake instability. Yet there are no experimental data on effects of gouge composition, and gouge confinement under combined high normal stress, water saturation and pore pressure. These conditions will be explored in future experiments.

METHODS SUMMARY

The present phase of the experiments included study of rate- and time-dependent friction on bare, solid blocks of Sierra White granite (supplied by ColdSprings). Each sample includes two cylindrical blocks 101.6 mm in diameter and 50.8 mm in height. The upper block has a raised ring structure with inner diameter of 63.2 mm and outer diameter of 82.3 mm (Supplementary Fig. 1d, e). The blocks were pressed against each other along the raised ring; the velocity at outer diameter is only about 14% higher than the velocity at the inner diameter. The deformation and heat generation in the sample were simulated in a finite-element model. The granite blocks are glued by epoxy to aluminium cylindrical grips, surface-ground

and roughened with 600 grit SiC powder. Thermocouples were cemented into holes drilled 3 mm and 6 mm away from the sliding surfaces (Supplementary Fig. 1). The normal stress σ_n was kept constant during a given experiment within the range 0.5 MPa to 7.1 MPa. The experimental run times ranged from 2 s (high velocity) to 3,000 s.

Full Methods and any associated references are available in the online version of the paper at www.nature.com/nature.

Received 19 December 2009; accepted 13 July 2010.

- Jordan, T. (committee chair) *Living on an Active Earth: Perspectives on Earthquake Science* (National Research Council, 2003).
- Dieterich, J. H. Modeling of rock friction. 1. Experimental results and constitutive equations. *J. Geophys. Res.* **84**, 161–162,–168 (1979).
- Dieterich, J. H. Constitutive properties of faults with simulated gouge. *Geophys. Monogr.* **24**, 103–120 (1981).
- Hirose, T. & Shimamoto, T. Slip-weakening distance of faults during frictional melting as inferred from experimental and natural pseudotachylytes. *Bull. Seismol. Soc. Am.* **95**, 1666–1673 (2005).
- Mizoguchi, K., Hirose, T., Shimamoto, T. & Fukuyama, E. Moisture-related weakening and strengthening of a fault activated at seismic slip rates. *Geophys. Res. Lett.* **33**, L16319, doi: 10.1029/2006GL026980 (2006).
- Ruina, A. Slip instability and state variable friction laws. *J. Geophys. Res.* **88**, 19359–19370 (1983).
- Di Toro, G., Goldsby, D. L. & Tullis, T. E. Friction falls towards zero in quartz rock as slip velocity approaches seismic rates. *Nature* **427**, 436–439 (2004).
- Beeler, N. M. & Tullis, T. E. Self-healing slip pulses in dynamic rupture models due to velocity dependent strength. *Bull. Seismol. Soc. Am.* **86**, 1130–1148 (1996).
- Marone, C. J. Laboratory-derived friction laws and their application to seismic faulting. *Annu. Rev. Earth Planet. Sci.* **26**, 643–696 (1998).
- Marone, C. J. Earthquake science—faults greased at high speed. *Nature* **427**, 405–406 (2004).
- Mair, K. & Marone, C. J. Friction of simulated fault gouge for a wide range of velocities and normal stresses. *J. Geophys. Res.* **104**, 28899–28914 (1999).
- Yund, R. A., Blanpied, M. L., Tullis, T. E. & Weeks, J. D. Amorphous material in high strain experimental fault gouges. *J. Geophys. Res.* **95**, 15589–15602 (1990).
- Scholz, C. H. *The Mechanics of Earthquakes and Faulting* 2nd edn (Cambridge Univ. Press, 2002).
- Lockner, D. A. *et al.* Geometry of the Nojima Fault at Nojima-Hirabayashi, Japan. I. A simple damage structure inferred from borehole core permeability. *Pure Appl. Geophys.* **166**, 1649–1667 (2009).
- Ben-Zion, Y. & Sammis, C. G. Characterization of fault zones. *Pure Appl. Geophys.* **160**, 677–715 (2003).
- Wilson, B., Dewers, T., Reches, Z. & Brune, J. Particle size and energetics of gouge from earthquake rupture zones. *Nature* **434**, 749–752 (2005).
- Brodsky, E. E. & Kanamori, H. Elastohydrodynamic lubrication of faults. *J. Geophys. Res.* **106**, 16,357–16,374 (2001).
- Byerlee, J. D. Frictional characteristics of granite under high confining pressure. *J. Geophys. Res.* **72**, 3639–3648 (1967).
- Beeler, N. M. & Tullis, T. E. Implications of Coulomb plasticity for the velocity dependence of experimental faults. *Pure Appl. Geophys.* **144**, 251–276 (1995).
- Wang, W. B. & Scholz, C. H. Wear processes during frictional sliding of rock—a theoretical and experimental study. *J. Geophys. Res.* **99**, 6789–6799 (1994).
- Worniyoh, E. Y. A., Jasti, V. K. & Higgs, C. F. A review of dry particulate lubrication: powder and granular materials. *J. Tribol.* **129**, 438–449 (2007).
- Binggeli, M. & Mate, C. M. Influence of water-vapor on nanotribology studied by friction force microscopy. *J. Vacuum Sci. Technol. B* **13**, 1312–1315 (1995).
- Muhuri, S. K., Dewers, T. A., Scott, T. E. & Reches, Z. Interseismic fault strengthening and earthquake-slip instability: friction or cohesion? *Geology* **31**, 881–884 (2003).
- Rabinowicz, E. The relation between friction and wear for boundary-lubricated surfaces. *Proc. Phys. Soc. Lond. B* **68**, 603–608 (1955).
- Godet, M. The 3rd-body approach—a mechanical view of wear. *Wear* **100**, 437–452 (1984).
- Higgs, C. F., Heshmat, C. A. & Heshmat, H. S. Comparative evaluation of MoS₂ and WS₂ as powder lubricants in high speed, multi-pad journal bearings. *J. Tribol.* **121**, 625–630 (1999).
- Heshmat, H. The quasi-hydrodynamic mechanism of powder lubrication. 3. On theory and rheology of triboparticulates. *J. Tribol.* **38**, 269–276 (1995).
- Ide, S. & Takeo, M. Determination of constitutive relations of fault slip based on seismic wave analysis. *J. Geophys. Res.* **102**, 27379–27391 (1997).
- Paterson, M. S. & Wong, T. F. *Experimental Rock Deformation—The Brittle Field* 347 (Springer, 2005).

Supplementary Information is linked to the online version of the paper at www.nature.com/nature.

Acknowledgements We thank J. Young, who built our instrument, as well as E. Eshkol, M. Hamilton, D. Moore, A. Madden, J. Chang and S. Busetti. Comments and reviews by J. Andrews, N. Beeler, C. Sammis, T.-f. Wong and J. Fineberg improved the manuscript. This study is supported by the National Science Foundation, Geosciences, Equipment and Facilities (grant number 0732715).

Author Contributions All authors made equal contributions to this study.

Author Information Reprints and permissions information is available at www.nature.com/reprints. The authors declare no competing financial interests. Readers are welcome to comment on the online version of this article at www.nature.com/nature. Correspondence and requests for materials should be addressed to Z.R. (reches@ou.edu) or D.A.L. (lockner@usgs.gov).

METHODS

We describe here the experimental set-up of our rotary friction apparatus and the wear-rate calculations.

Experimental set-up

General features. Our experimental system was funded by an NSF “Equipment and facilities” grant, and it was built by J. Young in the Department of Physics and Astronomy, University of Oklahoma. The system has the essential properties for the study of earthquake fault weakening: (1) the capability to apply normal stress up to 35 MPa, slip velocity of 0.001 to 2 m s⁻¹, rise-time to full velocity <0.1 s, and unlimited slip distance; (2) Continuous control of slip velocity without the need to periodically reverse the sense of slip⁷; (3) A ring design of the fault blocks with minor velocity difference (14%) between the outer and inner diameters, eliminating the need for the velocity corrections required for solid cylinders^{4,5}; and (4) high-frequency, up to 10 kHz, continuous monitoring of the laboratory fault behaviour, including measurement of normal load, shear load, slip velocity, displacement normal to the fault surface, and temperature.

Loading system. The apparatus frame is 1.8 m high with two massive decks (Supplementary Fig. 1a–c). The decks are connected to each other by four rectangle legs that are internally reinforced. The sample is placed between the two decks, and it is loaded by the rotary drive-train from below and by normal stress from above (Supplementary Fig. 1). The power system includes:

- (1) A 100 HP three-phase electric motor (Reliance) and controller (Baldor) that provide constant torque of up to 3,000 N m from 0 to 3,300 revolutions per minute, and which can accelerate to full speed in 0.1 s. The motor velocity is controlled and monitored through an 8192 line encoder.
- (2) The main rotation shaft is powered by the motor with 1:6 velocity reduction sprockets.
- (3) A 225-kg flywheel can boost motor torque.
- (4) A large electromagnetic clutch (Ogura) that is designed to fully engage within 30 ms.
- (5) A hydraulic piston system (Enerpac) with axial load up to 9,500 N and pneumatic accumulator.
- (6) Torque monitoring system (Supplementary Fig. 1a, b) designed to measure to shear stress in the gouge.

(Reference to commercial product names should not be construed as an endorsement. Rather, specific components are identified to provide a reference for independent determination of machine performance.)

Control and monitoring system. The control and monitoring system is based on National Instruments components, and includes a SCXI-1100 with modules 1124 (analogue control), 1161 (relay control), 1520 (load cell/strain gauge), and 1600 (data acquisition and multiplexer), as well as a USB-6210 for encoder measurements. We use LabView as the control software. Digital sampling rate is up to 10 kHz. Load-cells for axial load and torque are made by Honeywell, displacement normal to the fault surface is measured with four eddy-current sensors made by Lion’s Precision ($\pm 1 \mu\text{m}$ accuracy), temperature measurement is with thermocouples and infrared sensor (Omega), and sample angular velocity is monitored by a Sick–Stegmann encoder. We also monitor the motor velocity and motor torque through the channels of the Baldor controller.

Samples composition. The samples of the Sierra White granite were supplied by ColdSprings. The electron-microprobe modal analysis of Sierra White granite is comprised of six main minerals: plagioclase (48%), quartz (38%), alkali-feldspar (5%), ferromagnesian-mica (5%), and muscovite (5%) (Supplementary Fig. 2). Mean grain size is about 0.3 mm, mean void space in electron-microprobe images is ~4%.

Sample preparation. Each sample includes two cylindrical blocks 101.6 mm in diameter and 50.8 mm in height. The upper block has a raised ring structure with inner diameter of 63.2 mm and outer diameter of 82.3 mm (Supplementary Fig. 1d, e). The blocks were pressed against each other along the raised ring; the velocity at the outer diameter is only about 14% higher than the velocity at the inner diameter. The deformation and heat generation in the sample were simulated in a finite-element model, and presented here. The granite blocks are glued by epoxy to aluminium cylindrical grips, surface-ground and roughened with 600 grit SiC powder. Thermocouples were cemented into holes drilled 3 mm and 6 mm away from the sliding surfaces (Supplementary Fig. 1). The normal stress σ_n was kept constant during a given experiment within the range 0.5 to 7.1 MPa. The experimental run times ranged from 2 s (high velocity) to 3,000 s.

Wear and wear-rate calculations

Measuring wear. The common methods of wear measurements are by weighing wear products²⁰, measuring displacement normal to the sliding surfaces^{20,30,31}, or optical techniques. Each method has its limitations: weighing powder is time-consuming and it disrupts the structure of the fault. After a measurement, it is practically impossible to return to the previous stage. The optical methods are difficult to perform in situ, and require an accurate reference surface. Instead, we determine wear by continuously measuring the fault closure/opening with high precision ($\pm 1 \mu\text{m}$) sensors (see above).

Wear-rate calculations. We continuously monitored the change in closure/opening U , normal to the fault; positive U represents closure. The closure has three contributions: (1) surface wear W , indicated by closure ($U > 0$); (2) thermal expansion ($U < 0$) due to frictional heating; and (3) compaction ($U > 0$) or dilation ($U < 0$) of the gouge zone or the granite. We calculate the time-dependent wear-rate as follows. First, the thermal contribution is determined by using the temperature measured by the thermocouple embedded 3 mm from the sliding fault. We monitored the closure due to sample cooling after the sample stops, and used an empirical cooling–closure curve to determine the opening ($U < 0$) during shear. The validity of this procedure was tested by simulating frictional heat with a specially built ring heater that fits under the sliding ring and can heat the sample without fault motion. An example of temperature-corrected closure is shown in Supplementary Fig. 5. Once the gouge layer is established and its thickness is nearly constant, the excess gouge is ejected from the fault surface. Under this condition, the fault wear is approximately equal to the thermally adjusted closure, $W \approx U$. Thus, the wear is the thermally corrected closure (in μm).

Next, we fit a polynomial curve (order of 5–13) to the wear data (Supplementary Fig. 5) and take the derivative of this curve with respect to fault slip to obtain the dimensionless wear-rate dW/dx , where x is the fault-parallel slip. We use a simple, purely geometric unit:

$$\text{Experimental wear-rate} \equiv [\text{volume of wear products/area of sliding surfaces}] / [\text{slip distance}] \equiv [\text{thermally corrected closure}] / [\text{slip distance}]$$

There is no universal wear-rate unit; it can be dimensionless (m m^{-1} , namely metre per metre), or it can be $10^{-6} \text{m m}^{-1} = \mu\text{m m}^{-1}$, which is the one more suitable for experimental results and the one we use.

30. Hiratsuka, K. & Muramoto, K. Role of wear particles in severe–mild wear transition. *Wear* **259**, 467–476 (2005).
31. Hird, J. R. & Field, J. E. A wear mechanism map for the diamond polishing process. *Wear* **258**, 18–25 (2005).